Order by disorder in the classical Heisenberg *kagomé* antiferromagnet

Jan N. Reimers
Department of Physics, Simon Fraser University, Burnaby, British Columbia, Canada V5A 1S6

A. J. Berlinsky
Institute for Materials Research, McMaster University, 1280, Main Street West, Hamilton, Ontario, Canada L8S 4M1
(Received 9 October 1992; revised manuscript received 21 May 1993)

Antiferromagnetic ordering on a *kagomé* net is frustrated by the geometry of the lattice. The infinite number of classical ground states suggests that the system might not order at zero temperature, even for Heisenberg spins. However, high-temperature series expansions and earlier simulations indicate that this degeneracy is resolved by thermal fluctuations (i.e., order by disorder), suggesting a nine-sublattice coplanar Néel-like ordering of the spins. Coplanar nematic, random three-state Potts, and Néel orderings for the Heisenberg *kagomé* lattice antiferromagnet are investigated with Monte Carlo simulations coupled with state-of-the-art histogram methods for data analysis. We see strong evidence for thermal selection of long-range order with the spin correlations exhibiting algebraic decay, but the low-temperature phases are also seen to posses a *chiral* domain structure and very short-range chiral correlations. It is argued that the spin correlations are, surprisingly, rather insensitive to this lack of chiral order. Our results are consistent with $T=0$ being a critical point for this model system.

I. INTRODUCTION

Frustration in periodic spin systems is known to result in a number of diverse phenomena such as noncollinear[1] and helical[2] Néel-like ordering (i.e., sublattice ordering) as well as more subtle types of ordering such as nematic order[3,4] where the spins select a single axis or plane in spin space and orient themselves randomly within that submanifold. It has long been known that frustration due to lattice geometry in some Ising systems can result in infinite ground-state degeneracy and no long-range order at any temperature, the most famous example being the two-dimensional triangular-lattice antiferromagnet, for which the statistical mechanics was solved exactly by Wannier.[5] For vector spins (XY or Heisenberg) on a triangular lattice, the frustration is somewhat relieved and a noncollinear state forms with neighboring spins making angles of 120°. The fcc Ising antiferromagnet also has infinite ground-state degeneracy, but in this case thermal fluctuations select a long-range-ordered state at nonzero temperature.[6] This process of thermal fluctuations resolving a degeneracy is known as *ordering by disorder.*[7]

Even since Anderson proposed his resonating-valence-bond (RVB) theory of high-temperature superconductivity,[8] there has been intense interest in finding spin models and magnetic materials which exhibit spin-liquid behavior. Of these, the best studied are the $S=\frac{1}{2}$, J_1-J_2 square-lattice antiferromagnet[9] and the $S=\frac{1}{2}$ triangular-lattice antiferromagnet.[10] It is still not clear[11] whether the ground state of the triangular-lattice system is Néel-like with a large moment reduction[12] or spin-liquid-like with no sublattice order.[13] Other likely candidates for spin-liquid behavior are frustrated lattice models with highly degenerate classical ground states such as the *kagomé*- and pyrochlore-lattice antiferromagnets.

The kagomé lattice is a two-dimensional lattice of corner-sharing triangles (Fig. 1) and the pyrochlore lattice is a three-dimensional network of corner-sharing tetrahedra and is a natural three-dimensional (3D) analog of the kagomé lattice. Mean-field theory for these systems[14] predicts no long-range order, and both systems have infinite ground-state degeneracy[15,16] for Heisenberg

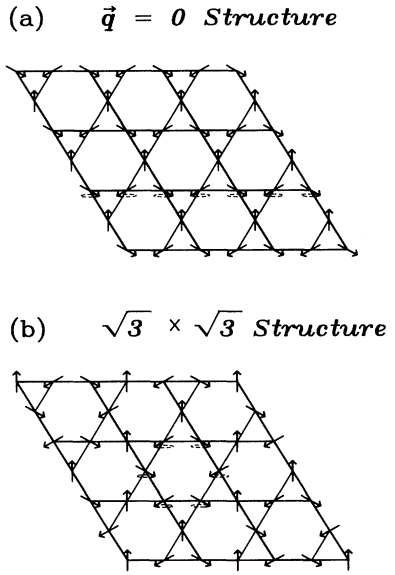

FIG. 1. Nine unit cells of the kagomé lattice showing (a) the $\mathbf{q}=\mathbf{0}$ and (b) the $\sqrt{3}\times\sqrt{3}$ Néel-like ground states. The dashed ellipses indicate possible spin rotations for each ground state that cost zero energy.

spins. The question remains as to whether the order-by-disorder mechanism will be effective in these systems. Even if thermal fluctuations select a subset of the ground-state manifold at low temperature, it is still not clear that this subset is restrictive enough to result in long-range Néel order. Of course, long-range order, which breaks a continuous symmetry, will only occur in the $T \to 0$ limit[17] for a 2D lattice model. Then the question of long-range order translates to the question, which of the infinitely many types of ground states has the largest Boltzmann weight or probability in the limit $T \to 0$? In general, the ground states with large Boltzmann weights will be the ones with the softest low-lying excitations.

Landau theory for the kagomé-lattice antiferromagnet predicts that an infinite number of zero modes, corresponding to all wave vectors in the first zone for one branch, becomes unstable below the mean-field critical temperature T_c^{MF}.[14] A zero mode is a collective motion of the spins that costs zero internal energy. A recent high-temperature series expansion[18] has shown that thermal fluctuations will not break this degeneracy, up to seventh order in J/T, where J is the exchange constant. Only at eight order does wave-vector selection occur, depending on the number of spin components, n. For XY ($n=2$) and Heisenberg ($n=3$) spins, the $\sqrt{3}\times\sqrt{3}$ phase [Fig. 1(b)] with $\mathbf{q}_{\sqrt{3}}=2\pi(\frac{2}{3},\frac{2}{3})$, is selected, and for the random-walk problem ($n=0$), the $\mathbf{q}=\mathbf{0}$ phase [Fig. 1(a)] is selected. Ising spins ($n=1$) do not select a wave vector at this or any[19] order in the series. Although the high-temperature series cannot predict any low-temperature properties with certainty, it does prove that the wave-vector degeneracy present at seventh order in J/T is *not* due to a fundamental symmetry of the system. Chubukov[20] has shown that quantum fluctuations will also lift the q-space degeneracy in the large-S (spin quantum number) limit, by proving that the $\mathbf{q}=\mathbf{0}$ and the $\sqrt{3}\times\sqrt{3}$ phases are both local energy minima. However, the relative stability of the two phases and the possibility of other local minima is still an open question in this context.

Low-temperature expansions[4] indicate that coplanar nematic order occurs through the order-by-disorder mechanism. In the harmonic approximation, all coplanar ground states are shown to have an entire branch of zero modes and no nocoplanar ground state has as many zero modes (at harmonic order) as the coplanar ground states. Hence coplanar states are selected at low temperature because they have the largest number of *soft* excitations. A saturation of the nearest- and next-nearest-neighbor planer nematic correlations as $T \to 0$ has been observed[4] in Monte Carlo (MC) simulations, thus supporting the low-temperature expansion result. No evidence of wave-vector selection was reported in Ref. 4. Further work[21] taking nonlinear interactions between the normal modes into account indicates that $\sqrt{3}\times\sqrt{3}$ order is thermally selected in the low-temperature regime.

Within the manifold of coplanar states, there are an infinite number of ground states, with all spins pointing along one of three directions mutually oriented at 120°, satisfying the minimum-energy condition for each triangle $\mathbf{S}_1+\mathbf{S}_2+\mathbf{S}_3=0$. Because each spin can be in one of three states, we will refer to these as three-state Potts-like ground states. The Potts-like ground states are for the most part random. The $\mathbf{q}=\mathbf{0}$ and $\sqrt{3}\times\sqrt{3}$ configurations are special members of this set of ground states because they are characterized by a single wave vector. For vector spins both the $\sqrt{3}\times\sqrt{3}$ and $\mathbf{q}=\mathbf{0}$ phases are *chiral* and therefore doubly degenerate.

The branches of zero modes mentioned above correspond in real space to the so-called *weathervane defect,*[22] where all spins in a hexagon can rotate about a common axis [Fig. 1(b)]. For a general Potts-like ground state, this rotation has zero cost in energy at order θ^2, where θ is the rotation angle; anharmonic forces provide a restoring force at order θ^4, thereby stiffening the modes. However, the $\sqrt{3}\times\sqrt{3}$ ground state has the special property that all neighboring spins for any hexagon are collinear and there is no restoring force to all orders in θ. The $\mathbf{q}=0$ ground state also has zero modes along straight lines [Fig. 1(a)] with no restoring force, but these are much fewer in number than the weathervane defects, which are localized. Based on this qualitative discussion, we expect that the $\mathbf{q}=\mathbf{0}$ and $\sqrt{3}\times\sqrt{3}$ ground states will have different Boltzmann weights and that of the two the $\sqrt{3}\times\sqrt{3}$ phase is more likely selected at low temperature.

Huse and Rutenberg[19] calculated spin-spin correlations at low temperatures, $T/J \approx 0.005$, and report correlations consistent with short-range $\sqrt{3}\times\sqrt{3}$ order that are approximately equal to the corresponding correlations of the three-state Potts model at $T=0$. When the spin-spin correlations are extrapolated to zero temperature, they are found to be significantly stronger than the three-state Potts correlations. Since the Boltzmann weights of all three-state Potts-like ground states are equal, this suggests that for Heisenberg spins the $\sqrt{3}\times\sqrt{3}$ ground state has a larger Boltzmann weight as $T \to 0$. They also show that the three-state Potts model is critical at $T=0$, and since the extrapolated Heisenberg correlations are stronger, they suggest that the Heisenberg model should exhibit true long-range $\sqrt{3}\times\sqrt{3}$ order.

Sachdev[23] has studied the classical and quantum spin cases at finite temperature using the so-called large-N expansion technique, which is the Sp(N) generalization of the Sp(1) Heisenberg Hamiltonian. For large N the $\sqrt{3}\times\sqrt{3}$ ground state is found to have the largest Boltzmann weight and the $\mathbf{q}=\mathbf{0}$ state the smallest, all random Potts ground states having intermediate stability. The correlation length of the $\sqrt{3}\times\sqrt{3}$ ordering was found to diverge exponentially as $T \to 0$, $\xi_{\sqrt{3}} \propto \exp(c/T)$.

The kagomé-lattice antiferromagnet is realized in a number of experimental systems. The second-layer ^{3}He adsorbed on graphite is believed to be an $S=\frac{1}{2}$ kagomé antiferromagnet.[15,24] This system shows no sharp features in the low-temperature heat capacity; however, two broad peaks are observed in C_H. $SrCr_{8-x}Ga_{4+x}O_{19}$ consists of alternating kagomé and triangular sheets of Cr^{3+} ($S=\frac{3}{2}$) ions and is nonstoichiometric with at least 15% of the Cr sublattice occupied by Ga.[25] Both ^{3}He and $SrCr_{8-x}Ga_{4+x}O_{19}$ exhibit diffuse neutron scattering over a wide temperature range and show no signs of

long-range magnetic order. The family of jarosites $M\mathrm{Fe}_3(\mathrm{OH})_6(\mathrm{SO}_4)_2$ ($M=\mathrm{H}_3\mathrm{O}$, Na, K, Rb, Ag, NH_4, Tl, Pb, and Hg) (Ref. 26) have layers of Fe^{3+} ($S=\frac{5}{2}$) spins forming kagomé sheets which stack in a cubic close-packed ($\cdots ABCABC\cdots$) fashion. Those members of the series that have been studied using neutron diffraction are found to order at finite temperature with the $\mathbf{q}=\mathbf{0}$ in plane structure,[27] presumably because of interplanar interactions. The hexagonal tungsten bronze form of FeF_3 consists of kagomé layers of Fe^{3+} which are stacked in a regular ($\cdots AAA\cdots$) fashion with no in-plane offset between layers. Long-range magnetic order of the $\mathbf{q}=\mathbf{0}$ sort occurs in this material[28] below $T_c=97$ K.

Our purpose here is to establish a connection between the low- and high-temperature theoretical results and elucidate the nature of any spin ordering that occurs as $T\rightarrow 0$ using the MC methods described in Sec. II. In particular, we attempt to determine if the wave-vector selection predicted by the high-temperature series persists at low temperature. MC methods are also useful for studying the nonperturbative intermediate-temperature regimes that have not yet been investigated. Simulations at high temperatures enable comparison with the series-expansion results. The spin configurations tend to freeze at low temperatures in MC simulations, so that only a small region of the low-energy phase space is sampled in finite-length simulations. In an attempt to overcome this problem, we have averaged the results of numerous simulations at low temperature, which gives a larger sampling of phase space and emulates a situation in which all degrees of freedom are, in principle, allowed to relax.

In our simulations we see a power-law decay of the correlation functions on finite-size lattices, indicating a tendency toward long-range order as $T\rightarrow 0$. However, the low-temperature ordering is not of the ideal $\sqrt{3}\times\sqrt{3}$ type. The ideal $\sqrt{3}\times\sqrt{3}$ structure also has long-range staggered chiral order which is unstable toward the formation of chiral domain walls. These domain walls form at no cost in internal energy, but do give a gain in entropy, at the expense of a stiffening of some of the soft modes. However, the chiral domain structure has a surprisingly small effect on the spin-spin correlations. Our results are consistent with $T=0$ being a critical point for this model system. A more detailed summary of our results and conclusions can be found in Sec. X.

The outline of the rest of the paper is as follows. Details of the MC methods used are described in Sec. II. The effects of the zero modes on some elementary thermodynamic functions are discussed in Sec. III, and results for nematic, chiral, and random Potts order parameters are presented in Sec. IV. Section V addresses the more difficult question of Néel ordering as $T\rightarrow 0$, followed by a brief discussion of the long relaxation times at low temperatures in Sec. VI. The decay of some correlation functions and the predicted powder neutron-scattering patterns at various temperatures are described in Sec. VII. The chiral domain structure and its effects on the spin-spin correlations are discussed in Sec. VIII. A comparison with the high-temperature series results in Sec. IX is followed by summary and conclusions in Sec. X.

II. MONTE CARLO METHOD

A standard isotropic classical spin Hamiltonian

$$\mathcal{H}=\frac{1}{2}J\sum_{\mathbf{R},a}\sum_{\tau}\mathbf{S}(\mathbf{R}+\mathbf{r}_a)\cdot\mathbf{S}(\mathbf{R}+\mathbf{r}_a+\tau) \tag{1}$$

was simulated, where $\mathbf{R}$ is a lattice vector, $\mathbf{r}_a$ is a sublattice vector for sublattice a, τ is a nearest-neighbor bond vector, $\mathbf{S}=(S_x,S_y,S_z)$ is a unit three-vector, and $J>0$ is the nearest-neighbor antiferromagnetic exchange constant. System sizes $L=6$, 12, 18, and 24 unit cells with periodic boundary conditions were considered. The number of spins, $N=3L^2$, ranged from 108 to 1728. Simulation lengths were 10 000 MC steps per spin at each temperature and covered many decades in temperature, $0.002\leq T/J\leq\infty$. We define one MC step as one attempted spin move for every spin in the lattice. Because of the large number of temperatures simulated and our use of the histogram method of data analysis (to be described below), the *effective* number of MC steps at each temperature is actually much larger than 10 000. Some simulations at temperatures as low as $T/J=0.0005$ were performed in order to calculate spin-correlation functions. Random spin moves were attenuated by a factor δ; i.e., a random $\Delta\mathbf{S}$ is replaced by $\delta\Delta\mathbf{S}$ and $0\leq\delta\leq 1$. δ was adjusted in such a way that on average 50% of the attempted spins moves were accepted. This was important at low temperatures. When a spin move was rejected, the spin was then randomly pivoted around its local exchange field.[29] Such pivoting has no effect on the internal energy, but does increase the rate at which phase space is sampled.

All thermodynamic quantities were calculated using multiple-histogram methods.[30] The multiple-histogram method makes optimal use of all data because probability distributions, or histograms, generated by MC at a given temperature contain information on distributions at nearby temperatures through the reweighting transformation[30]

$$P_{\beta'}(E_\nu)=\frac{P_\beta(E_\nu)\exp[(\beta-\beta')E_\nu]}{\sum_\mu P_\beta(E_\mu)\exp[(\beta-\beta')E_\mu]}\ . \tag{2}$$

Here $P_{\beta'}(E_\nu)$ is the probability of the system having energy E_ν at inverse temperature $\beta'=(k_B T')^{-1}$, which is calculated in (2) from the probability distribution at a different temperature β. Because of this sharing of information between simulations at different temperatures, the *effective* number of MC steps at each temperature is much larger than the 10 000 steps actually simulated. This extra information is discarded in conventional MC methods. In total, 131 temperatures for each lattice size were simulated and combined using the multiple-histogram method.[30] Equilibrium spin configurations for one temperature were used as starting configurations for the next nearby temperature, and 1000 MC steps were allowed to reach equilibrium after each temperature change. Cooling runs were initiated with a random-spin configuration at $T/J=\infty$, and warming runs were initiated with both the $\mathbf{q}=\mathbf{0}$ and $\sqrt{3}\times\sqrt{3}$ ground states. Unless otherwise specified, data presented below are cal-

culated starting from a random-spin configuration at $T=\infty$ and systematically annealed. All runs (warming and cooling) were repeated between 50 and 100 times, and the data were combined by adding the histograms for each temperature. A complete cooling run from $T/J=\infty$ down to $T/J=0.002$ involved $\approx 10^8$ MC steps per spin, which corresponds to $\approx 2.5\times 10^{11}$ attempted spin flips for a 24×24 unit-cell lattice.

Another feature of the histogram method is that information on the temperature dependence of the partition function, and hence the free energy, is automatically provided. Strictly speaking, the partition function is only determined to within an arbitrary multiplicative factor

$$\mathcal{Z}_{\text{true}}=\mathcal{Z}_{\text{MC}}\exp(\Delta S/k_B) \tag{3}$$

or

$$\mathcal{F}_{\text{true}}=\mathcal{F}_{\text{MC}}-T\Delta S \tag{4}$$

and

$$S_{\text{true}}=\frac{E-\mathcal{F}_{\text{MC}}}{T}+\Delta S\ . \tag{5}$$

Hence the MC method determines the entropy to within an arbitrary additive constant, which we determine by fixing the entropy at $T=\infty$ to $S_{\text{true}}(T=\infty)=k_B\ln(4\pi)$ per spin. Calculating the absolute entropy at low temperatures requires overlapping histograms over the whole temperature range from $T=\infty$ down to the desired low temperature.

III. COUNTING ZERO MODES

As Chalker, Holdsworth, and Shender[4] have pointed out, modes with harmonic restoring forces contribute $\frac{1}{2}k_BT$ to the internal energy and anharmonic modes (θ^4) contribute $\frac{1}{4}k_BT$, where k_B is Boltzmann's constant. For a single unit cell of a kagomé system in one of its coplanar ground states, there are six transverse modes, of which one has a quartic (θ^4) restoring force, which leads to an internal energy per spin of

$$E=E_0+\tfrac{11}{12}k_BT+O(T^2)\ , \tag{6}$$

where $E_0/J=-1$ is the energy per spin for any three-state Potts ground state. The zero-temperature heat capacity is therefore $\frac{11}{12}k_B$ per spin. As the heat capacity, derived from energy fluctuations by MC simulations at low temperature, is rather noisy, we prefer to test this mode counting by inspecting the internal energy and entropy. Similar arguments to the one above predict that the low-temperature entropy per spin will be dominated by a logarithmic singularity as $T\to 0$,

$$S=\tfrac{11}{12}k_B\ln(T/J)+O(1)\ . \tag{7}$$

Figure 2 shows extrapolation to $T=0$ of the quantity $(E-E_0)/T$ for various lattice sizes cooled from high temperature. The agreement is to within less than 1% of $\frac{11}{12}$. The entropy, with the expected logarithmic singularity in (7) subtracted, is shown in Fig. 3, for $L=6$ and 24. The $L=12$ and 18 data are very similar to the $L=24$ results. The remaining entropy after subtraction still shows linear behavior as a function of $\ln(T/J)$ in the range $0.01\le T\le 0.1$. Next to each straight-line fit, we show the measured slope plus $\frac{11}{12}$, which corresponds to the actual $\ln(T/J)$ coefficient in (7). For $L=6$ two linear regimes are clearly seen. In the temperature range $0.01\le T/J\le 0.1$, the entropy behaves like $\ln(T/J)$, which is consistent with all six modes having a quadratic restoring force and therefore the system is not yet fully coplanar. A trend toward the expected low-temperature behavior in the entropy $[S=\frac{11}{12}\ln(T/J)]$ only starts to

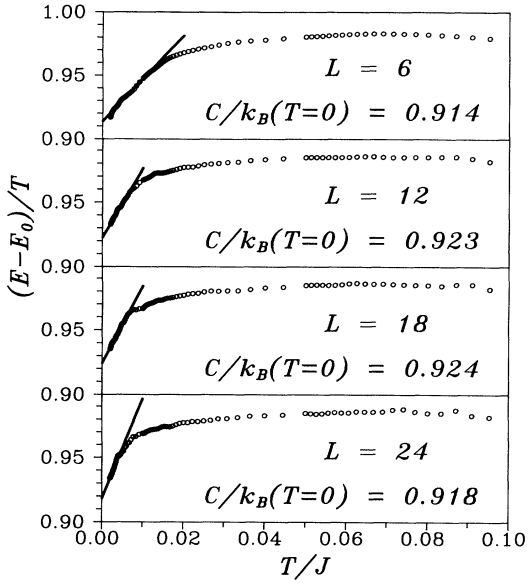

FIG. 2. Extrapolation of the heat capacity to zero temperature for the four lattice sizes studied. The expected theoretical limit is $C/k_B(T=0)=\frac{11}{12}\approx 0.917$.

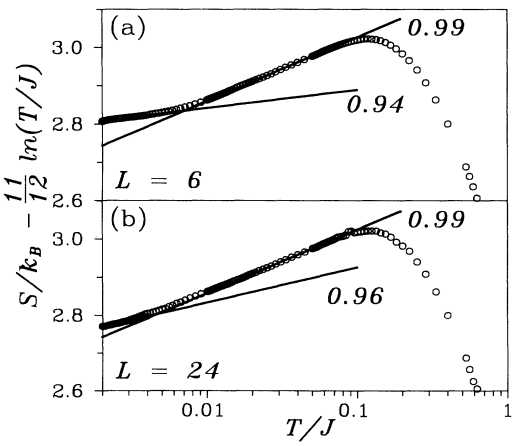

FIG. 3. Low-temperature behavior of the entropy for two lattice sizes (a) $L=6$ and (b) $L=24$. The temperature axis is on a logarithmic scale. Numbers next to the straight-line fits indicate the coefficient of the $\ln(T/J)$ term in the entropy, as obtained from the slope. These slopes are slightly larger than the expected low-temperature limiting value of $\frac{11}{12}\approx 0.917$.

occur for $T/J<0.01$, depending on the lattice size. The decrease in the $\ln(T/J)$ coefficient below 1 can be interpreted as a sign of the onset of coplanar ordering.

IV. NEMATIC AND CHIRAL ORDER

Nematic order can be characterized in a general manner with tensor order parameters which make no assumption about the selected spin plane. However, in order to simultaneously collect information on chirality, we prefer to look at the normal vector[4] to each elementary triangle of spins,

$$\mathbf{n}=\frac{2}{3\sqrt{3}}(\mathbf{S}_1\times\mathbf{S}_2+\mathbf{S}_2\times\mathbf{S}_3+\mathbf{S}_3\times\mathbf{S}_1)\ , \tag{8}$$

where $\mathbf{S}_1$, $\mathbf{S}_2$, and $\mathbf{S}_3$ belong to the same triangle. When the three spins form a coplanar 120° ground state, $\mathbf{n}$ points above or below the spin plane (depending on chirality) and $\mathbf{n}\cdot\mathbf{n}=1$. Here we use the convention that the chirality is $+1$ when the spins rotate clockwise in 120° increments as one traverses around the triangle clockwise. Also note that collinear normal vectors correspond to coplanar spins.

We have calculated the chiral correlation function

$$C_{n1}(\mathbf{r}-\mathbf{r}')=\langle\mathbf{n}_\mathbf{r}\cdot\mathbf{n}_{\mathbf{r}'}\rangle\ , \tag{9a}$$

the nematic correlation function

$$C_{n2}(\mathbf{r}-\mathbf{r}')=\tfrac{3}{2}\langle(\mathbf{n}_\mathbf{r}\cdot\mathbf{n}_{\mathbf{r}'})^2\rangle-\tfrac{1}{2}\ , \tag{9b}$$

and their corresponding susceptibilities

$$T\chi_{ni}=\sum_\mathbf{r} C_{ni}(\mathbf{r})\ ,\quad i=1,2\ . \tag{10}$$

The summation here is over triangles (not lattice sites). Throughout we will always plot radial correlation functions $C(|\mathbf{r}-\mathbf{r}'|)$, with any angular dependence on $\mathbf{r}$ averaged over. C_{n1} and χ_{n1} are sensitive to the $\mathbf{q}=\mathbf{0}$ phase where all triangular plaquettes have the same chirality. For random Potts-like ground states that are close to the $\mathbf{q}=\mathbf{0}$ phase in structure, we expect χ_{n1} to be large. In the $\sqrt{3}\times\sqrt{3}$ phase, the normal vectors order antiferromagnetically and we expect $C_{n1}(r)$ to be rapidly oscillating and $\chi_{n1}\approx 0$. On the other hand, χ_{n2} is insensitive to chirality and only indicates whether or not the spin configuration is coplanar. In the same spirit as above, we have also calculated the *staggered* chiral correlation function and its corresponding susceptibility,

$$C^{\mathrm{St}}_{n1}(\mathbf{r}-\mathbf{r}')=\langle\mathbf{n}_\mathbf{r}\cdot\mathbf{n}_{\mathbf{r}'}\rangle\exp(i[\omega_\mathbf{r}-\omega_{\mathbf{r}'}])\ , \tag{11}$$

and

$$T\chi^{\mathrm{St}}_{n1}=\sum_\mathbf{r} C^{\mathrm{St}}_{n1}(\mathbf{r})\ , \tag{12}$$

where $\omega_\mathbf{r}=0$ if the triangle at $\mathbf{r}$ is pointing up and $\omega_\mathbf{r}=\pi$ for down-pointing triangles. For random Potts-like ground states that are close to the $\sqrt{3}\times\sqrt{3}$ phase in structure, we expect χ^{St}_{n1} to be large.

The two chiral susceptibilities are shown in Figs. 4(a) and 4(b). χ_{n1} is small at all temperatures, while χ^{St}_{n1} grows logarithmically at lower temperatures. χ^{St}_{n1} shows no obvious lattice-size dependence, indicating that the staggered chiral correlations are short range. There appears to be no long-range chiral order of the varieties considered here. The nematic susceptibility χ_{n2} [Fig. 4(c)] also grows at low temperature and is much larger in magnitude than either of the chiral susceptibilities. This indicates that the normal vectors at least line up in collinear fashion as Chalker, Holdsworth, and Shender have suggested.[4] The strong dependence of χ_{n2} on lattice size below $T/J\approx 0.004$ is clear evidence that the nematic correlations are long range at these temperatures compared to $r/a_{\mathrm{cell}}\approx 24$. χ_{n2} has essentially two temperature regimes. As T/J is reduced from 1.0 to 0.01, the normal vectors are growing in magnitude (as seen from $\langle|\mathbf{n}|\rangle$, not shown) and are relatively unaligned. In the range $0.002\le T/J\le 0.01$, the normal vectors have essentially attained unit magnitude and tend to line up in a collinear fashion which corresponds to a coplanar spin state. For the largest lattice ($L=24$), coplanar order only starts to set in below $T/J=0.004$. This is seen clearly in Fig. 5(a) where the nematic correlation function $C_{n2}(r)$ for an 18×18 lattice becomes long-range ordered below $T=0.005$, indicating that the nematic correlation length $\xi_{n2}/a_{\mathrm{cell}}>18$, where a_{cell} is the lattice constant. The apparent long-range order at nonzero temperature is an artifact of the periodic boundary conditions and the finite lattice. The inset in Fig. 5(a) shows the rapidly oscillating

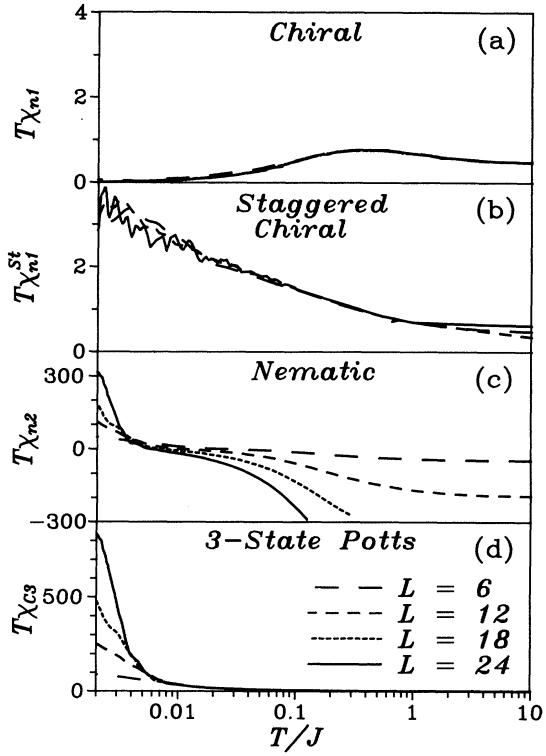

FIG. 4. (a) Uniform and (b) staggered chiral susceptibilities χ_{n1} and χ^{St}_{n1}, (c) nematic susceptibility χ_{n2}, and (d) the random three-state Potts susceptibility χ_{C_3}. The temperature axis is on a logarithmic scale.

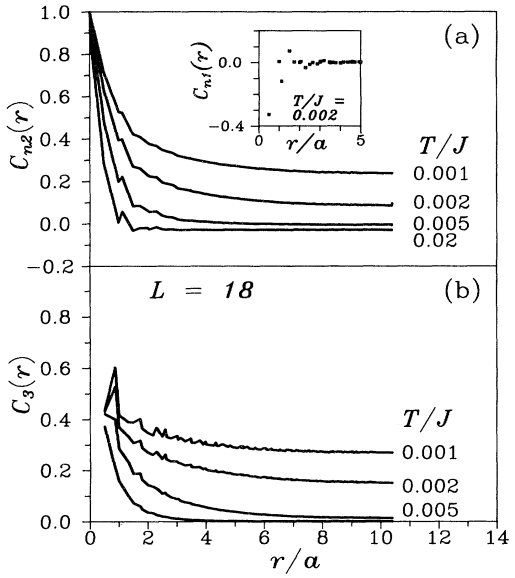

FIG. 5. Radial correlation functions for (a) the nematic ordering $C_{n2}(r)$ and (b) the random three-state Potts ordering $C_3(r)$ at four temperatures. The inset in (a) shows the short-range chiral correlations $C_{n1}(r)$ at $T/J=0.002$.

nature of $C_{n1}(r)$ and the rapid decay of chiral correlation strength with distance at the lowest temperature considered. Beyond about three lattice spacings, all chiral correlations average to zero within statistical errors. Huse and Rutenberg have pointed out that the chiral correlations in the three-state Potts model at zero temperature have a very strong power-law decay[19] with distance like $r^{-\eta}$ with $\eta=4$. They could not measure such a strong decay in their simulations. It is not clear if this result also holds for the Heisenberg problem; if it does, we also cannot measure the decay.

The nematic order parameters are not sensitive to the 120° ordering that we expect to take place in the coplanar state. Labeling the angular coordinates of the spins as $\Omega=(\theta,\phi)$, we define the correlation function

$$C_l(\mathbf{r}-\mathbf{r}')=\left[\frac{4\pi}{2l+1}\right]\sum_{m=-l}^{l}\langle Y_l^m(\Omega)Y_l^{m*}(\Omega')\rangle \ , \tag{13}$$

where Ω and Ω' are directions of the spins at $\mathbf{r}$ and $\mathbf{r}'$, respectively, and $Y_l^m(\Omega)$ is a spherical harmonic. In a coordinate system where the z axis in spin space is perpendicular to the plane spanned by $\mathbf{S}_\mathbf{r}$ and $\mathbf{S}_{\mathbf{r}'}$, we have

$$Y_l^l(\Omega)Y_l^l(\Omega')+Y_l^{-l}(\Omega)Y_l^{-l}(\Omega')\propto\cos(l\phi_{\mathbf{r},\mathbf{r}'}) \ ,$$

where $\phi_{\mathbf{r},\mathbf{r}'}$ is the angle between the two spins. Summing over m yields a scalar invariant, which is largest when the angle between $\mathbf{S}_\mathbf{r}$ and $\mathbf{S}_{\mathbf{r}'}$ is some multiple of $2\pi/l$. For $l=3$, Eq. (13) will be the order parameter for any 120° coplanar state, independent of the orientation of the plane in spin space. Using the summation of spherical harmonics theorem, we have

$$C_l(\mathbf{r}-\mathbf{r}')=\langle P_l(\mathbf{S}_\mathbf{r}\cdot\mathbf{S}_{\mathbf{r}'})\rangle \ , \tag{14}$$

where P_l is a Legendre polynomial. In particular,

$$C_l(\mathbf{r}-\mathbf{r}')=\langle \mathbf{S}_\mathbf{r}\cdot\mathbf{S}_{\mathbf{r}'}\rangle \tag{15}$$

is the normal spin-spin correlation function,

$$C_2(\mathbf{r}-\mathbf{r}')=\tfrac{1}{2}[3\langle(\mathbf{S}_\mathbf{r}\cdot\mathbf{S}_{\mathbf{r}'})^2\rangle-1] \tag{16}$$

is sensitive to collinear spin ordering [see Eq. (9b)], and

$$C_3(\mathbf{r}-\mathbf{r}')=\tfrac{1}{2}[5\langle(\mathbf{S}_\mathbf{r}\cdot\mathbf{S}_{\mathbf{r}'})^3\rangle-3\langle\mathbf{S}_\mathbf{r}\cdot\mathbf{S}_{\mathbf{r}'}\rangle] \tag{17}$$

is the correlation function for all three-state Potts-like ground states. The three correlation functions just described, as well as their corresponding susceptibilities

$$T\chi_{C_l}=\sum_{\mathbf{r}}C_l(\mathbf{r}) \ , \tag{18}$$

have been calculated. χ_{C_3} and $C_3(r)$ are shown in Figs. 4(d) and 5(b), respectively, and are consistent with long-range three-state Potts-like order below $T=0.005$ for $L=18$. Similar to χ_{n2} we see that χ_{C_3} appears to be diverging as $T\to0$ and the strong lattice-size dependence again indicates long-range order for the lattice sizes considered. A more detailed analysis of these correlation functions will appear below once the $\sqrt{3}\times\sqrt{3}$ correlation function has been introduced. The results for the nematic ordering are in good agreement with the low-temperature expansion and MC results of Chalker, Holdsworth, and Shender. Below we will address the more difficult question of wave-vector selection and Néel ordering.

V. NÉEL ORDER

We have shown that coplanar ordering, with all spins pointing along one of three possible directions in a plane, takes place at temperatures below $T/J\approx0.01$ for finite lattices ($L\leq24$). There are an infinite number of these 3 three-state Potts-like ground states, and here we will try to determine whether or not some subclass of these states is selected over the others. This question is difficult to answer with MC methods due to the freezing in of certain degrees of freedom at low temperatures. Moving from one Potts state to another involves the simultaneous rotation of a large number of spins. The weathervane rotation is the most likely as it involves only six spins; however, this mode only occurs when there is local $\sqrt{3}\times\sqrt{3}$ order. In general, loops larger than the elementary hexagon must be simultaneously rotated in order to sample all degrees of freedom. An algorithm which finds loops and rotates them with a Metropolis acceptance scheme should work, but for simplicity we have chosen to average the data from a number of cooling runs as described in Sec. II.

Order parameters and susceptibilities were calculated for the $\mathbf{q}=\mathbf{0}$ phase,

$$\langle m_0\rangle=\langle\sqrt{\mathbf{m}_0\cdot\mathbf{m}_0^*}\rangle \ , \tag{19}$$

$$\langle m_0^2\rangle=\langle\mathbf{m}_0\cdot\mathbf{m}_0^*\rangle \ , \tag{20}$$

$$T\chi_0=N(\langle m_0^2\rangle-\langle m_0\rangle^2) \ , \tag{21}$$

where

$$\mathbf{m}_0=\frac{1}{N}\sum_{\mathbf{R},\mathbf{r}_a}\mathbf{S}(\mathbf{R}+\mathbf{r}_a)\exp(i\phi_a)\ , \tag{22}$$

N is the number of lattice sites, and the ϕ_a are sublattice phase angles, $\phi_1=0$, $\phi_2=2\pi/3$, and $\phi_3=4\pi/3$. Similar quantities $m_{\sqrt{3}}$ and $\chi_{\sqrt{3}}$ were calculated for the $\sqrt{3}\times\sqrt{3}$ phase where

$$\mathbf{m}_{\sqrt{3}}=\frac{1}{N}\sum_{\mathbf{R},\mathbf{r}_a}\mathbf{S}(\mathbf{R}+\mathbf{r}_a)\exp(i\mathbf{q}_{\sqrt{3}}\cdot[\mathbf{R}+\mathbf{r}_a])\ , \tag{23}$$

and $\mathbf{q}_{\sqrt{3}}=2\pi(\frac{2}{3},\frac{2}{3})$ is the $\sqrt{3}\times\sqrt{3}$ ordering wave vector. Our wave vectors refer to the standard crystallographic unit cell for which the **a** and **b** real-space basis vectors, which subtend an angle of 120°, are represented by (1,0) and (0,1), respectively.

The two order parameters are shown in Fig. 6 where it is clearly seen that the $\sqrt{3}\times\sqrt{3}$ ordering is favored. The $\sqrt{3}\times\sqrt{3}$ order parameter fluctuations, $T\chi_{\sqrt{3}}$ for the largest lattice size (Fig. 7), have power-law behavior with two distinct temperature regimes. Above $T/J=0.01$ where the system tends to a coplanar state, we see that $T\chi_{\sqrt{3}}\approx T^{-0.3}$. Below $T/J=0.01$ where the $\sqrt{3}\times\sqrt{3}$ order parameter starts to grow, the divergence of the fluctuations becomes much stronger, $T\chi_{\sqrt{3}}\approx T^{-\gamma}$ [$\gamma=1.24(5)$]. The corresponding fluctuations in $m_0, T\chi_0$, are more than an order of magnitude smaller. This strongly suggests that the system goes critical at $T=0$ and that $m_{\sqrt{3}}$ is the correct order parameter.

The theory of finite-size scaling for critical phase transitions at finite temperature is now rather well developed and tested. Such finite-size scaling assumes power-law

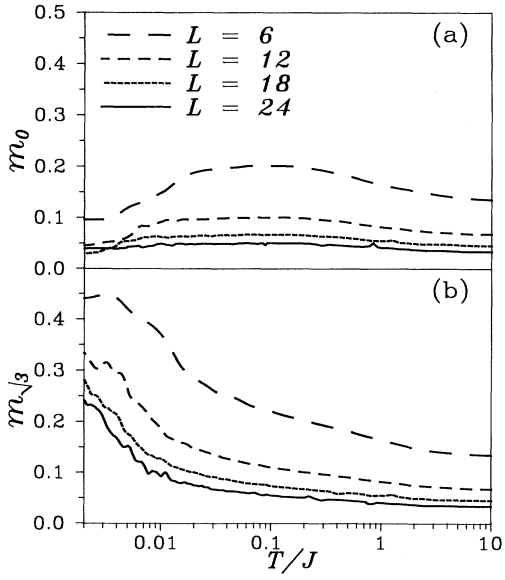

FIG. 6. Root-mean-square order parameters (a) m_0 for the $\mathbf{q}=\mathbf{0}$ and (b) $m_{\sqrt{3}}$ for the $\sqrt{3}\times\sqrt{3}$ Néel ordered phases for four lattice sizes. The temperature axis is on a logarithmic scale.

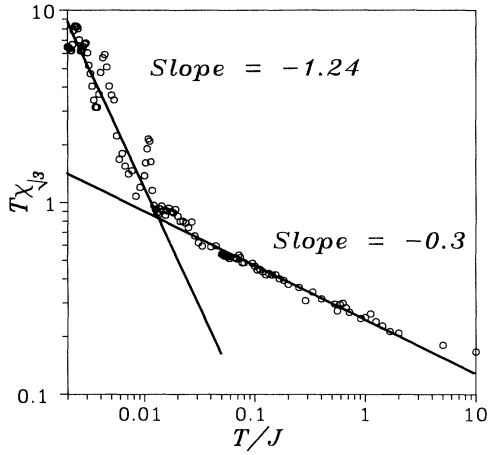

FIG. 7. Mean-squared fluctuations of the $\sqrt{3}\times\sqrt{3}$ order parameter showing two power-law regimes and a possible divergence as $T\to 0$.

divergence of the correlation length and the ordering susceptibility. One might argue that the low-temperature properties of the Heisenberg kagomé antiferromagnet should instead be like those of the 2D classical Heisenberg ferromagnet (2D CHF). The 2D CHF is known to exhibit long-range order at $T=0$ and exponential divergences in the susceptibility and the correlation length.[31] Standard finite-size scaling theory for critical points does *not* apply to systems such as the 2D CHF (which are related to the nonlinear σ model). However, because of the soft modes and the unusual chiral domain structure (to be discussed below), we would argue that the critical properties of the Heisenberg kagomé antiferromagnet are fundamentally different than those of the 2D CHF and perhaps different from other known critical points. Here we proceed with the assumption that the power-law divergences of $\chi_{\sqrt{3}}$ and algebraic decay of the spin-spin correlations (see below) indicate that $T=0$ is a critical point and hence that finite-size scaling is applicable. In the absence of any better theory, we will attempt to scale our order parameter data according to the standard theory of finite-size scaling,[32]

$$m_{\sqrt{3}}L^{\beta/\nu}=\mathcal{f}(L^{1/\nu}T)\ , \tag{24}$$

where β and ν are critical exponents, L is the lattice size, and $\mathcal{f}$ is a nonuniversal scaling function. In practice, the critical exponents must be determined by trial and error in such a way that the data in the critical region, for all lattice sizes, collapse onto a single line $\mathcal{f}(x)$. Figure 8 shows our best attempt at scaling the data, yielding very approximate critical exponents $\beta\approx 0.3(1)$ and $\nu\approx 1.0(2)$. The data noise is too severe to allow a more accurate determination of the exponents. The asymptotic behavior for $\mathcal{f}(x)$,[33]

$$\mathcal{f}(x)\approx x^{\beta-d\nu/2}\ ,\ \text{large } x\ , \tag{25}$$

where d is the lattice dimensionality, provides a further check of the exponents. The asymptotic slope (Fig. 8) gives $\beta-\nu=-0.6$, which is consistent with $\beta\approx 0.3(1)$

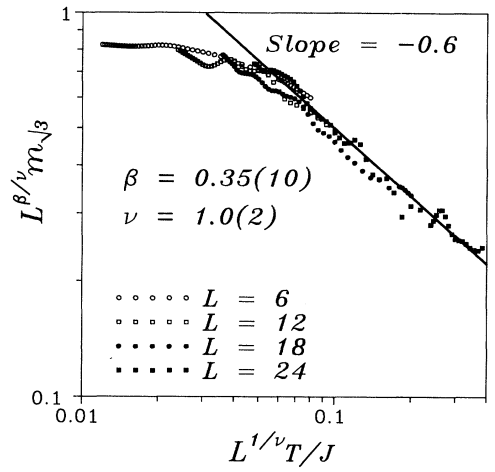

FIG. 8. Finite-size scaling analysis for the $\sqrt{3}\times\sqrt{3}$ order parameter $m_{\sqrt{3}}$ at low temperature. The exponents β and ν were chosen such that the data for all lattice sizes collapse, as well as possible, onto a single line.

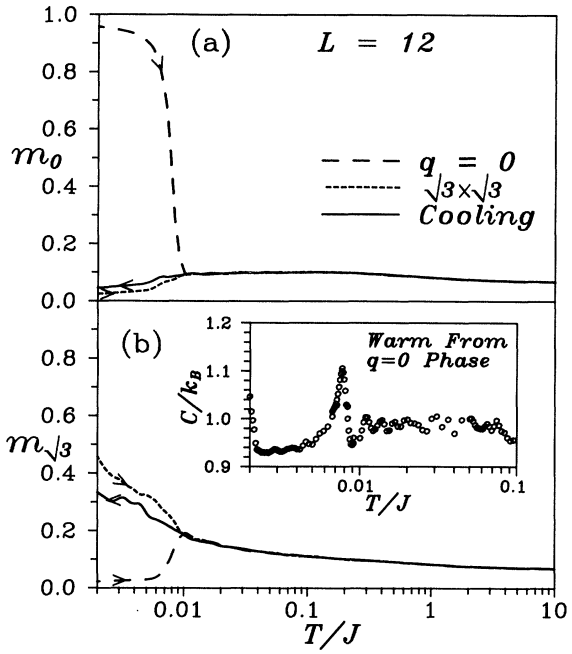

FIG. 9. Comparison of the order parameter (a) m_0 and (b) $m_{\sqrt{3}}$ for warming runs from the $\mathbf{q}=\mathbf{0}$ and $\sqrt{3}\times\sqrt{3}$ ground states and cooling from a random configuration at $T=\infty$. The inset in (b) shows the heat capacity for the warming run from the $\mathbf{q}=\mathbf{0}$ ground state. The temperature axis is on a logarithmic scale.

and $\nu\approx 1.0(2)$, within the estimated error. The exponents β, ν, and γ are also consistent with the scaling relations $\alpha+2\beta+\gamma=2$ and $d\nu=2-\alpha$, if $\alpha\approx 0$. The objective here is merely to show that the data can scale as expected for a critical order parameter and not to determine accurate exponents. An accurate determination of the exponents (assuming $T=0$ is a critical point) would require extremely long simulation times and most certainly larger lattices.

Further insight is gained by comparing m_0 and $m_{\sqrt{3}}$ as the system is warmed, from both the $\mathbf{q}=\mathbf{0}$ and the $\sqrt{3}\times\sqrt{3}$ ground states, with the results obtained from slow cooling. m_0 and $m_{\sqrt{3}}$ are shown in Figs. 9(a) and 9(b), respectively. Here 50 000 MC steps were allowed for the ground-state configurations to relax. A discussion of the validity of this relaxation time will be given in Sec. VI. The cooling data are intermediate between the data for warming from the two ground states, but much closer to the $\sqrt{3}\times\sqrt{3}$ warming results. When warming from the $\mathbf{q}=\mathbf{0}$ ground state, $m_{\sqrt{3}}$ and m_0 jump to their cooling values near $T/J=0.008$, suggesting that the $\mathbf{q}=\mathbf{0}$ phase is really out of equilibrium. This is confirmed by the sharp feature in the heat capacity [inset Fig. 9(b)] at the same temperature. No such feature occurs when cooling or warming from the $\sqrt{3}\times\sqrt{3}$ configuration. Also, we see that m_0 remains rather large when warming from the $\mathbf{q}=\mathbf{0}$ ground state, while $m_{\sqrt{3}}$ decays from 1 to ≈ 0.5 during the relaxation time. This effect is presumably due to the larger number of soft modes in the $\sqrt{3}\times\sqrt{3}$ ground state.

If the $\sqrt{3}\times\sqrt{3}$ state really has a larger Boltzmann weight than the $\mathbf{q}=\mathbf{0}$ phase, then it should also have a higher entropy at low temperatures. In Fig. 10 the entropy difference $\Delta S=S_{\sqrt{3}}-S_0$ is shown for two lattice sizes $L=6$ and 12. As stated previously, accurate calculation of the low-temperature absolute entropy with the MC method is very difficult and requires data with good statistics over a very wide temperature range. We are looking at very subtle effects, and the entropy differences here are on the order of 0.3% of the absolute entropy below $T/J=0.01$. Nevertheless, a definite entropy

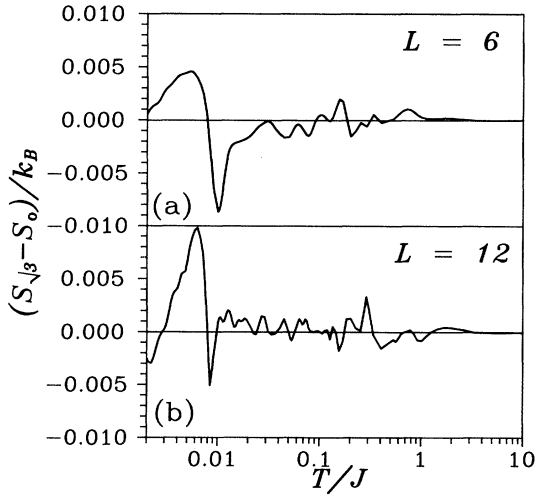

FIG. 10. Entropy difference between runs warming from the $\mathbf{q}=\mathbf{0}$ and $\sqrt{3}\times\sqrt{3}$ ground states for lattice sizes (a) $L=6$ and (b) $L=12$. The peak in the temperature range $0.003\le T/J\le 0.008$ indicates that the $\sqrt{3}\times\sqrt{3}$ phase has higher entropy than the $\mathbf{q}=\mathbf{0}$ phase. The temperature axis is on a logarithmic scale.

difference below $T/J=0.01$, consistent with the $\sqrt{3}\times\sqrt{3}$ phase having higher entropy, can be seen and the effect seems to become more pronounced for the larger lattice size, except at the very lowest temperature. The dip in ΔS at $T=0.01$ is an artifact of the phase change that occurs at that temperature [see inset Fig. 9(b)] while warming from the $\mathbf{q}=\mathbf{0}$ state.

VI. RELAXATION

Figure 9(b) shows that $m_{\sqrt{3}}$ decays from 1 to ≈ 0.5 during the relaxation time of 50 000 MC steps. It is natural to ask if 50 000 MC steps is really long enough and also if lattice size has an effect on the relaxation. The time dependence, over 6.5 decades in MC time, of $m_{\sqrt{3}}$ at $T/J=0.002$ and three lattice sizes ($L=6,12,24$) is shown in Fig. 11. The $L=6$ lattice relaxes abruptly after 10 000 MC steps, and $L=12$ relaxes less abruptly after about 70 000 MC steps. Thus, for the warming runs from the $\sqrt{3}\times\sqrt{3}$ ground state after the 50 000-MC-step relaxation time, the system is about 95% equilibrated with regards to $\sqrt{3}\times\sqrt{3}$ order. Our data at the two very lowest temperatures simulated ($J/T=500$ and 490) may be slightly perturbed by this, but none of our basic conclusions will be. The behavior of the $L=24$ lattice is rather different and seems to show a fast decay regime $5000\le t\le 100\,000$ and slower decay in the range $100\,000\le t\le 6\,000\,000$. Even after 6×10^6 MC steps, it is not clear that $m_{\sqrt{3}}$ has equilibrated; a very slow decay in $m_{\sqrt{3}}$ may still be taking place. The spin configuration for the 24×24 lattice run was saved after 10^6 and 6×10^6 MC steps and used to calculate some correlation functions and investigate chiral ordering.

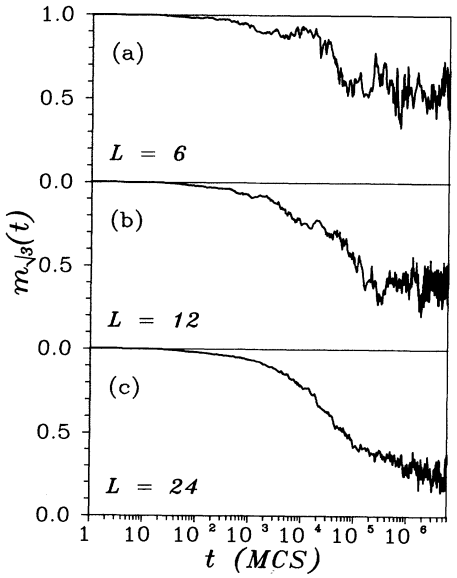

FIG. 11. Relaxation of the $\sqrt{3}\times\sqrt{3}$ order parameter $m_{\sqrt{3}}$ as a function of MC time for three lattice sizes (a) $L=6$, (b) $L=12$, and (c) $L=24$. The time axis is on a logarithmic scale.

VII. CORRELATIONS AND NEUTRON SCATTERING

Out of the infinite number of three-state Potts-like ground states, our attention until now has been focused on only two, the $\mathbf{q}=\mathbf{0}$ and the $\sqrt{3}\times\sqrt{3}$ ground states. It seems rather clear at this point that the $\sqrt{3}\times\sqrt{3}$ ground state is (a) definitely favored over the $\mathbf{q}=\mathbf{0}$ state and (b) also shows some tendency toward being naturally selected upon cooling. These conclusions are based on the following results:

(1) The staggered chiral susceptibility, which is consistent with $\sqrt{3}\times\sqrt{3}$ ordering, is growing at low temperatures and is always larger than the uniform chiral susceptibility.

(2) The order parameter $m_{\sqrt{3}}$ grows and is naturally selected on cooling at low T, while m_0 gets very small as $T\to 0$.

(3) The order parameter fluctuations $\chi_{\sqrt{3}}$ show an apparent power-law divergence and $\chi_{\sqrt{3}}\gg\chi_0$.

(4) There is a similarity between the order parameters for cooling runs and runs warming from the $\sqrt{3}\times\sqrt{3}$ ground state.

(5) There is a phase transition observed while warming from the $\mathbf{q}=\mathbf{0}$ state, indicating it is really out of equilibrium (metastable) at low temperature.

(6) There is a slightly larger entropy for the $\sqrt{3}\times\sqrt{3}$ phase at low temperature.

There still lurks the possibility that ordered states characterized by wave vectors other than $\mathbf{q}=(0,0)$ and $\mathbf{q}=2\pi(\frac{2}{3},\frac{2}{3})$ may show an equal or stronger tendency to be selected. The selection of a *small* number of other "mystery" wave vectors seems unlikely because $\mathbf{q}=\mathbf{0}$ and $\mathbf{q}=\pm 2\pi(\frac{2}{3},\frac{2}{3})$ are the only wave vectors consistent with a 120° spin arrangement that is observed in the $C_3(r)$ correlation function. Any of the random three-state Potts-like ground states will be characterized by a distribution of wave vectors (or Fourier modes) and will not fall into the above category, but such random 120° structures are the most likely alternatives to the $\sqrt{3}\times\sqrt{3}$ ordering.

We have calculated the correlation function for $\sqrt{3}\times\sqrt{3}$ ordering,

$$C_{\sqrt{3}}(\mathbf{r})=\frac{\langle \mathbf{S}_0\cdot\mathbf{S}_r\rangle}{\cos(\mathbf{q}_{\sqrt{3}}\cdot\mathbf{r})}\ , \tag{26}$$

which is equal to unity for all $\mathbf{r}$ when the spins are in the $\sqrt{3}\times\sqrt{3}$ configuration. The $\sqrt{3}\times\sqrt{3}$ correlation function becomes positive definite for all $\mathbf{r}$ on an 18×18 lattice below $T/J=0.01$, which is similar to the behavior of the three-state Potts correlation function $C_3(r)$ except that the strength of the correlations in $C_{\sqrt{3}}(r)$ are much weaker. All correlation functions studied except the chiral correlations seemed to exhibit power-law decay with distance

$$C(r)\propto r^{-\eta} \tag{27}$$

at temperatures below $T/J\approx 0.01$, as exemplified by the data for $T/J=0.002$ in Fig. 12. For comparison, we have also included the correlations obtained from a 24×24 lattice (Sec. VI) that was allowed to relax from the $\sqrt{3}\times\sqrt{3}$ ground state for 10^6 MC steps and then

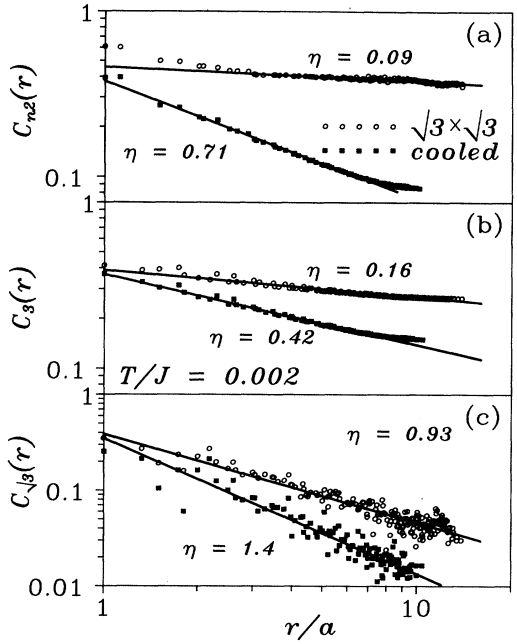

FIG. 12. Power-law decay of three correlation functions (a) $C_{n2}(r)$, (b) $C_3(r)$, and (c) $C_{\sqrt{3}}(r)$ at $T/J=0.002$ for systems cooled from $T=\infty$ and relaxed from the $\sqrt{3}\times\sqrt{3}$ ground state. Straight-line fits yield estimates for the critical exponents η.

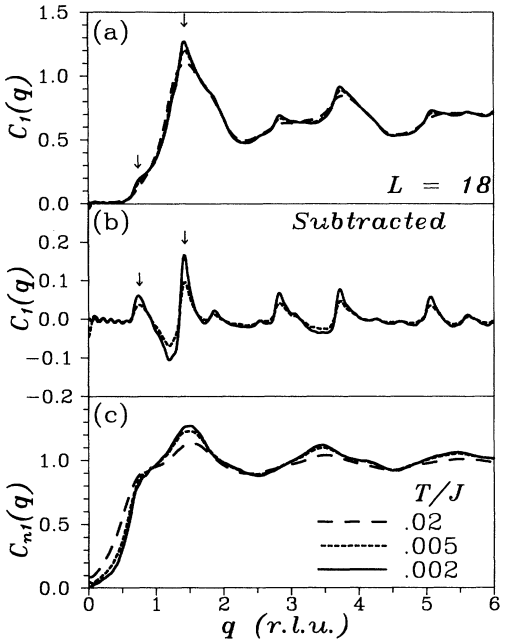

FIG. 13. (a) Powder-averaged magnetic structure factor $C_1(q)$ at three temperatures for $L=18$. (b) $C_1(q)$ for the two lowest temperatures with the diffuse scattering at $T/J=0.02$ subtracted. Arrows indicate expected Bragg angles for the $(\frac{1}{3},\frac{1}{3})$ and $(\frac{2}{3},\frac{2}{3})$ magnetic reflections from the $\sqrt{3}\times\sqrt{3}$ phase. (c) Fourier transform of the chiral correlation function $C_{n1}(q)$ showing only broad features which grow in intensity but do not narrow as the temperature is lowered.

averaged over 10^5 MC steps. All three correlation functions decay much more rapidly for the annealed system, indicating that one or possibly both of these configurations are not really at equilibrium, the truth being somewhere in between. Hence the data in Fig. 12 may be thought of as representing lower and upper bounds on the true equilibrium correlation functions. The power-law decay with distance, of $C_{n2}(r)$, $C_3(r)$, and most notably $C_{\sqrt{3}}(r)$, suggests long-range order for these finite lattice sizes, i.e., $\xi/a_{\text{cell}} \gg L$.

In order to check for other ordering wave vectors, we have calculated the radial Fourier transform of the spin-spin correlations $C_1(r)$,

$$C_1(q)=\frac{1}{N}\sum_r N_r\langle \mathbf{S}_0\cdot\mathbf{S}_r\rangle\frac{\sin(2\pi qr)}{2\pi qr}\ , \tag{28}$$

where angular degrees of freedom in $\mathbf{q}$ have been integrated out and N_r is the number of spins at distance r. For a short-range-ordered system, this is similar to what is observed in a powder neutron-diffraction experiment. The Fourier transforms for an 18×18 lattice cooled from high temperature are shown in Fig. 13(a) for three averaging temperatures $T/J=0.02$, 0.005, and 0.002. At $T/J=0.02$ no sharp features are present, which is consistent with neutron-diffraction experiments by Broholm *et al.*,[25] the high-temperature series expansion,[18] and Gaussian approximation calculations.[34] Arrows indicate the angles where one expects to see the $(\frac{1}{3},\frac{1}{3})$ and the $(\frac{2}{3},\frac{2}{3})$ Bragg reflections from the $\sqrt{3}\times\sqrt{3}$ structure. Indeed, there does seem to be some intensity increase at these wave vectors, which is most clearly seen in Fig. 13(b) where the diffuse data from $T/J=0.02$ have been subtracted. All peaks in Fig. 13(b) can be indexed with reciprocal-lattice points corresponding to the $\sqrt{3}\times\sqrt{3}$ structure. The asymmetric peak shape is a standard feature of powder-averaged scattering from any two-dimensional ordered system.

We have compared our $\sqrt{3}\times\sqrt{3}$ spin correlations with those of the three-state Potts model in its ground state as calculated by Huse and Rutenberg.[19] We find that at $T/J=0.002$ the correlations for an annealed 24×24 lattice are essentially identical to the corresponding three-state Potts values. However, for a 24×24 lattice that was relaxed from the $\sqrt{3}\times\sqrt{3}$ ground state for 6×10^6 MC steps, the spin correlations are noticeably stronger than the three-state Potts values. We were unable to make a connection between the annealed and relaxed systems. Conventional MC methods seem incapable of establishing, in a simulation of reasonable length, what the equilibrium spin correlations are at this low temperature. As the spin correlations obtained after relaxing for 10^6 MC steps were essentially identical to those obtained after 6×10^6 steps, it seems that little progress will be made with even longer simulations. All we can say is that the truth lies somewhere in between our relaxed and annealed simulations. Hence we cannot verify that the Huse-Rutenbergs extrapolated ($T\to0$) spin correlations are really correct. This is an important question because

their argument—that true long-range order (i.e., a nonzero order parameter as opposed to $T=0$ being a critical point with $m_{\sqrt{3}}=0$) occurs at $T=0$—relies on the fact that the $(T\rightarrow 0)$ spin correlations are stronger than the corresponding three-state Potts correlations.

As mentioned in the Introduction, both the $\mathbf{q}=\mathbf{0}$ and $\sqrt{3}\times\sqrt{3}$ ground states are chiral. Every triangle in the $\mathbf{q}=\mathbf{0}$ structure has the same chirality, i.e., all + or all −. For a $\sqrt{3}\times\sqrt{3}$ state, up-pointing triangles have opposite chirality to down-pointing, triangles. Hence $\sqrt{3}\times\sqrt{3}$ ordering implies antiferromagnetic ordering of the normal vectors $\mathbf{n}_{\mathbf{r}}$ defined in Eq. (8). If the chiral ordering is long range, we expect sharp peaks in the Fourier transform of the chiral correlation function $C_{n1}(r)$, which is shown in Fig. 13(c). No such sharp features occur. The intensity of the broad peak at $q\approx 1.33$ grows as temperature is lowered, but does not become narrow like the peaks in $C_{\sqrt{3}}(q)$. $C_{n1}(q)$ is reminiscent of a liquid-structure factor. We obtain the same result for systems that are allowed to relax from the $\sqrt{3}\times\sqrt{3}$ ground state, even at temperatures as low as $T/J=0.0005$. This suggests that the strength of near-neighbor chiral correlations is growing, but the range of correlations remains very short and temperature independent. We know from the long-range correlations in $C_{n2}(r)$ that the normal vectors are somewhat collinear [Fig. 12(a)], which means that the short-range chiral order is not only due to nematic spin waves, but must also be due to chiral domain walls. How can $\sqrt{3}\times\sqrt{3}$ correlations be long range in the absence of long-range chiral ordering? We will address this question in the next section.

VIII. CHIRAL DOMAIN STRUCTURE

In order to describe the nature of the thermally selected ground states of the Heisenberg kagomé antiferromagnet, we must first introduce some nomenclature. We introduced the notion of chirality in Sec. IV, with the convention that +1 chirality corresponds to spins around a triangle rotating clockwise by 120° increments as one traverses clockwise around the triangle. The $\sqrt{3}\times\sqrt{3}$ ground state is doubly degenerate due to chirality, and because neighboring triangles have opposite chirality, the normal vectors are ordered antiferromagnetically. We will label the $\sqrt{3}\times\sqrt{3}$ ground state in which all up-pointing triangles have +1 chirality and all down-pointing triangles have −1 chirality, as the + chiral $\sqrt{3}\times\sqrt{3}$ ground state. Correspondingly, in the − chiral $\sqrt{3}\times\sqrt{3}$ ground state all up-pointing triangles have −1 chirality and all down-pointing triangles have +1 chirality. The + and − $\sqrt{3}\times\sqrt{3}$ ground states have wave vectors $+\mathbf{q}_{\sqrt{3}}$ and $-\mathbf{q}_{\sqrt{3}}$, respectively.

In Fig. 14(a) we show a snapshot of the system where the chirality of each triangle is marked (black triangles have chirality +1). This snapshot is for a 24×24 lattice system (discussed in Sec. IV) that was relaxed from the $\sqrt{3}\times\sqrt{3}$ ground state for 10^6 MC steps at $T/J=0.002$. The $-\mathbf{q}_{\sqrt{3}}$ chiral domains, with all down-pointing triangles black, have been shaded for clarity. The system is roughly an equal mixture of both $+\mathbf{q}_{\sqrt{3}}$ and $-\mathbf{q}_{\sqrt{3}}$ chiral domains, which corresponds to the highest-entropy situation with respect to the relative concentrations. Small domains in which a whole hexagon of triangles alternates chirality are very common and correspond to a weathervane defect with the six spins on the hexagon rotated by roughly 180°.

The chiral domain walls in Fig. 14(a) cost zero internal energy. An example is shown in Fig. 14(b) where all spins and the chirality of each triangle are shown. A chiral domain wall is indicated by the dashed line. Within each domain neighboring triangles have opposite chirality. Along the chiral domain wall, neighboring triangles have the same chirality. Also note that all spins

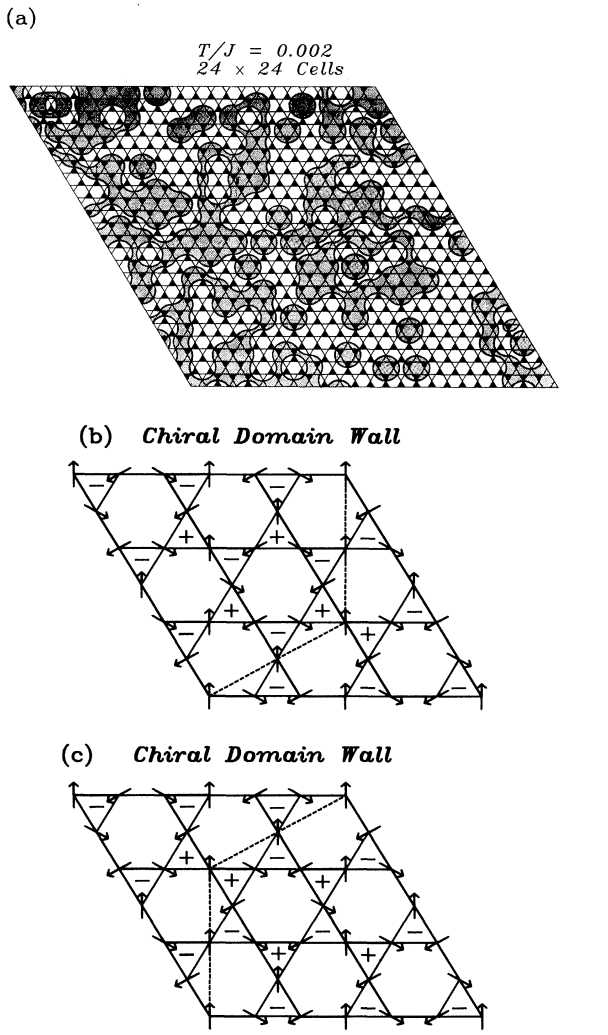

FIG. 14. (a) Schematic view of the chiral domain structure on a 24×24 lattice with periodic boundary conditions at $T/J=0.002$. The system was allowed to relax from the $\sqrt{3}\times\sqrt{3}$ ground state for 10^6 MC steps. Here +1 chirality triangles are shaded black and domains of − chiral order are shaded grey. (b) Schematic view of a $\sqrt{3}\times\sqrt{3}$ ground state with the chirality of each triangular plaquette indicated. A chiral domain wall is indicated by the dashed line. (c) As in (b) except the domain wall has moved as a result of a 180° weathervane rotation of the spins on the central hexagon.

which reside on the domain wall are collinear and simultaneously make 120° angles with all neighbors. No 120° antiferromagnetic nearest-neighbor bonds are violated; hence, the domain wall costs zero internal energy. By performing a 180° weathervane rotation of the six spins in the central hexagon in Fig. 14(b), the domain wall can be moved to a new location shown in Fig. 14(c). This is an example of domain-wall motion that has zero internal activation energy. This implies that the domain walls are never static, but will fluctuate at arbitrarily low temperatures. The wall motion does, however, involve spin rotation out of the thermally selected spin plane. Also, because entropy prefers equal amounts of + and − chiral domains, the domain walls at low concentration actually have a negative free energy. At high concentrations the opposite should be true since soft modes in the neighborhood of a domain wall will be stiffened by the wall.

Each chiral domain can also be labeled by a phase angle ϕ_ν, which takes on one of three distinct values $\phi_1=0$, $\phi_2=2\pi/3$, and $\phi_3=4\pi/3$ and corresponds to 120° spin rotations within a chiral domain. Hence there are actually six domain types labeled by $(\sigma\mathbf{q}_{\sqrt{3}},\sigma\phi_\nu)=(+,1)$, $(+,2)$, $(+,3)$, $(-,1)$, $(-,2)$, and $(-,3)$. We can now write down a general expression for spin directions in any domain (spins are in the XY plane):

$$\mathbf{S}(\mathbf{r},\sigma,\nu)=(\cos[\sigma(\mathbf{q}_{\sqrt{3}}\cdot\mathbf{r}+\phi_\nu)]\ ,\sin[\sigma(\mathbf{q}_{\sqrt{3}}\cdot\mathbf{r}+\phi_\nu)]\ ,0)\ , \tag{29}$$

where the position vector is $\mathbf{r}=\mathbf{R}+\mathbf{r}_a$, $\mathbf{R}$ being a lattice vector and $\mathbf{r}_a$ being the coordinates of sublattice a within a unit cell. In general, the spin-spin correlations

$$\mathbf{S}(\mathbf{r},\sigma,\nu)\cdot\mathbf{S}(\mathbf{r}',\sigma',\nu')=\cos[\mathbf{q}_{\sqrt{3}}\cdot(\sigma\mathbf{r}-\sigma'\mathbf{r}')+\sigma\phi_\nu-\sigma'\phi_{\nu'}] \tag{30}$$

will be affected by the chiral domain structure. If spin waves are for the moment ignored, then the thermal average of (30) is equivalent to averaging over domain types (σ,ν) and (σ',ν'), since the chiral domain walls are constantly fluctuating. For example, fixing $\mathbf{S}(\mathbf{r},\sigma,\nu)$ and assuming all domain types (σ',ν') are equally probable at distance $|\mathbf{r}-\mathbf{r}'|$, the average over ν' is strictly zero, independent of σ'. As we shall argue below, at any finite distance the domain types are not all equally probable and some spin-spin correlations will survive.

There appear to be short-range forces acting on the chiral structure as exemplified by the short-distance correlations in $C_{n1}(r)$ [Fig. 5(a) inset]. The chiral domain structure at short distances is clearly governed by some nontrivial rules. Below we will employ a simplified model which we call the "statistical model," which ignores all chiral correlations beyond first neighbor. This grossly overcounts the number of allowed states, as dictated by the 120° rule for all nearest-neighbor spins. We use the statistical model as a worst-case scenario and argue that $\sqrt{3}\times\sqrt{3}$ spin correlations will survive even in this crude approximation. If $\sqrt{3}\times\sqrt{3}$ spin correlations survive within the statistical model, then they must certainly survive when stronger (and more realistic) antichiral correlations are present.

The lattice of up-pointing triangles in a kagomé net is a triangular lattice. This triangular lattice can be randomly decorated with equal numbers of black and white triangles, corresponding to +1 and −1 chirality for each triangle. We can also associate black triangles with occupied sites in a percolation problem. A typical chiral domain structure can now be generated by choosing all down-pointing triangles to have opposite chirality to the nearest up-pointing triangle directly below it. Each down-pointing triangle has three neighboring up-triangles, and our particular choice of pairing each down triangle with the up triangle below it is arbitrary and introduces an artificial symmetry breaking into the model. Although a more general algorithm may exist, we believe our simple but arbitrary choice will have no effect on the final conclusions. This restriction on the down-pointing triangles results in a nearest-neighbor chiral correlation of strength $\frac{1}{3}$ as observed in the inset in Fig. 5(a). The prescription for random decoration ignores weak further neighbor short-distance forces acting on the chiral correlations. Within the statistical model, every up triangle has equal probability of being either of +1 or −1 chirality, regardless of the surrounding up-triangle configuration. Hence all chiral correlations $C_{n1}(r)$ are zero except for the nearest-neighbor ones. Our simulations indicate that the statistical model is valid at large distance r. However, the predicted power-law decay r^{-4} for the staggered chiral correlations for the three-state Potts model at zero temperature may also hold for the Heisenberg problem. As stated previously, our MC data cannot measure such a strong decay if it exists. Weak long-distance chiral correlations if present will have the effect of enhancing $\sqrt{3}\times\sqrt{3}$ order. Hence our following argument showing that $\sqrt{3}\times\sqrt{3}$ spin correlations can survive in the absence of chiral correlations (statistical model) is actually a worst-case scenario.

The statistical model is equivalent to the percolation problem on a triangular lattice. At half filling ($\frac{1}{2}$ black triangles), the triangular lattice is exactly at the $L=\infty$ percolation threshold. In a percolation problem, the probability of two lattice sites being in the same domain is described by the pair-connectedness function[35]

$$c(p,r)=\frac{\exp(-r/\xi_p)}{r^{d-2+\eta_p}}\ , \tag{31}$$

where p is the fraction of occupied sites, ξ_p is the correlation length which diverges near the percolation threshold p_c, and η_p is a percolation critical exponent. For our problem $d=2$, $p_c=\frac{1}{2}$, and[35] $\eta_p=\frac{5}{24}$, which leads to a power-law decay $c(p_c,r)\propto r^{-\eta_p}$. Hence, for the kagomé-lattice problem, the probability that any two spins are in the same chiral domain also has a power-law decay with distance, $c(\frac{1}{2},r)\propto r^{-\eta_p}$. Because $p=p_c$ and $\xi_p=\infty$, there is no natural length scale in the system and chiral domains of all sizes will exist. Also, the domain walls of large chiral clusters will be fractal.

The knowledge borrowed from percolation theory is

sufficient to draw some definitive conclusions regarding the effects of chiral domains on the spin-spin correlations. To begin with, we split the thermal (domain) average of (30) (still neglecting spins waves) into two terms, the first dealing with spin correlations between spins in the *same* chiral domain and a second term treating interdomain correlations. Without loss of generality, we can choose $\nu=1$ and $\sigma=+$,

$$\langle \mathbf{S}(\mathbf{r},+,1)\cdot\mathbf{S}(\mathbf{r}',\sigma',\nu')\rangle = \cos[\mathbf{q}_{\sqrt{3}}\cdot\Delta\mathbf{r}]c(p,\Delta r)+[1-c(p,\Delta r)]\sum_{\sigma',\nu'} w_{\nu}^{\sigma'}\cos[\mathbf{q}_{\sqrt{3}}\cdot(\mathbf{r}-\sigma'\mathbf{r}')-\sigma'\phi_{\nu}] , \tag{32}$$

where $\Delta\mathbf{r}=\mathbf{r}-\mathbf{r}'$ and the pair-connectedness function from percolation theory has been used. The interdomain (second) term contains a summation over all six possible domain types with corresponding weights $w_{\nu}^{\sigma'}$ for each type. The weights are functions of distance, Δr, and for notational convenience this will be implied throughout. By symmetry the weights for domains of opposite chirality are all equal, $w_1^- = w_2^- = w_3^-$. Similarly, $w_2^+ = w_3^+$, yielding

$$\begin{aligned}\sum_{\sigma',\nu'} w_{\nu}^{\sigma'}\cos[\mathbf{q}_{\sqrt{3}}\cdot(\mathbf{r}-\sigma'\mathbf{r}')-\sigma'\phi_{\nu}] \\ = w_1^+\cos[\mathbf{q}_{\sqrt{3}}\cdot\Delta\mathbf{r}]+w_2^+(\cos[\mathbf{q}_{\sqrt{3}}\cdot\Delta\mathbf{r}+\tfrac{2}{3}\pi]+\cos[\mathbf{q}_{\sqrt{3}}\cdot\Delta\mathbf{r}-\tfrac{2}{3}\pi])+w_1^-\sum_{\nu'}\cos[\mathbf{q}_{\sqrt{3}}\cdot(\mathbf{r}+\mathbf{r}')+\phi_{\nu}] \\ = \cos[\mathbf{q}_{\sqrt{3}}\cdot\Delta\mathbf{r}](w_1^+ - w_2^+) .\end{aligned} \tag{33}$$

Hence domain averaging destroys correlations between spins in domains of opposite chirality. We can now substitute the result (33) into (32),

$$\langle \mathbf{S}(\mathbf{r},+,1)\cdot\mathbf{S}(\mathbf{r}',\sigma',\nu')\rangle = \cos[\mathbf{q}_{\sqrt{3}}\cdot\Delta\mathbf{r}]\{c(p,\Delta r)+[1-c(p,\Delta r)][w_1^+(\Delta r)-w_2^+(\Delta r)]\} . \tag{34}$$

It is possible that intradomain correlations (first term in parentheses) will be partially canceled by the interdomain correlations (second term). We should note at this point that the $\sqrt{3}\times\sqrt{3}$ correlation function defined in (26) is a measure of the quantity in parentheses in (34) if spin waves are neglected. We have seen that (26) is positive definite at low temperatures, implying that the interdomain correlations do not exactly cancel the intradomain correlations.

To further check this, we have calculated the intra- and interdomain correlations separately at $T/J=0.002$ averaged over 10^6 MC steps for two lattice sizes $L=12$ and 24. The results are shown in Fig. 15. The intradomain correlations are positive definite, while interdomain correlations are always negative definite. However, at large distances the interdomain correlations are about a factor of 5 smaller in magnitude than the intradomain correlations for both lattice sizes. This lends strong support to our contention that interdomain correlations do *not* cancel the intradomain correlations.

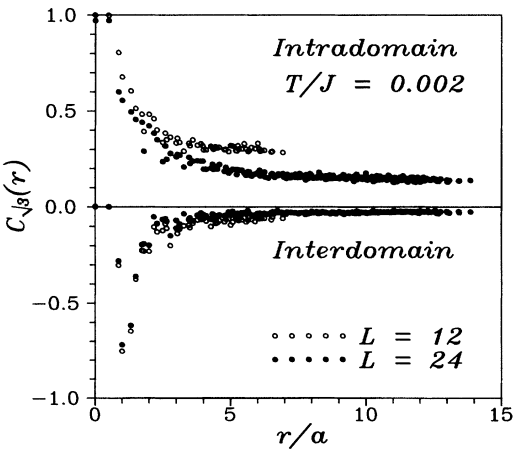

FIG. 15. Intradomain (top) and interdomain (bottom) $\sqrt{3}\times\sqrt{3}$ spin correlations for a 24×24 lattice at $T/J=0.002$ averaged over 10^6 MC steps. At large distances the interdomain correlations do not cancel the intradomain correlations.

To summarize, at low temperature the Heisenberg kagomé antiferromagnet exhibits a chiral domain structure and chiral correlations appear to be destroyed at large r. Because the chiral domain structure maps onto a triangular lattice at its percolation threshold, the chiral domains have no natural length scale. Domains of arbitrarily large size will exist. The chiral domain structure attenuates the spin-spin correlations with a power-law decay, but does *not* destroy the correlations. Our discussion so far has assumed no spin waves, which will be discussed next.

The $\sqrt{3}\times\sqrt{3}$ correlations will also be attenuated by spin waves. The spin waves will be of two sorts: spin waves which rotate the spins within the thermally selected spin plane and nematic spin waves which rotate spins out of the spin plane. Because the coplanar spin structure is thermally selected, the nematic spins waves will be much softer than the in-plane spin waves and therefore more populated at low temperatures. The spin-correlation decay will be a product of the percolation (chiral domain) and spin-wave decay functions which are both power laws in the limit $T\to0$,

$$C_{\sqrt{3}}(r)\propto r^{-(\eta_p+\eta_{\mathrm{SW}})} . \tag{35}$$

Hence the $\sqrt{3}\times\sqrt{3}$ correlations are still long range in the $T\to0$ limit. Our data in Fig. 12 indicate that

$$0.93\le\eta_p+\eta_{\mathrm{SW}}\le1.4 , \tag{36}$$

and we know from percolation theory that $\eta_p = \frac{5}{24} \approx 0.21$. Then, since $0.7 \leq \eta_{SW} \leq 1.2$, the nematic spin waves therefore dominate the decay of the spin-spin correlation function at low temperatures.

IX. COMPARISON WITH HIGH-TEMPERATURE SERIES

As pointed out in the Introduction, the high-temperature series-expansion work of Harris, Kallin, and Berlinsky[18] has shown that the mean-field wave-vector degeneracy of the free energy is broken, at eight order in J/T, by thermal fluctuations. The ordering wave vector $\mathbf{q}_{\sqrt{3}}$ was determined by looking at the wave-vector-dependent susceptibility

$$\chi_{ab}(\mathbf{q}) = \sum_{\mathbf{R}} \langle \mathbf{S}(\mathbf{r}_a)\cdot\mathbf{S}(\mathbf{R}+\mathbf{r}_b)\rangle \exp[-i\mathbf{q}\cdot(\mathbf{R}+\mathbf{r}_b-\mathbf{r}_a)] , \tag{37}$$

where, as before, a and b are sublattice indices. Maximizing the largest eigenvalue of $\chi(\mathbf{q})$ with respect to $\mathbf{q}$ determines the ordering wave vector. The maximal eigenvalue $\lambda_1(\mathbf{q})$ is independent of $\mathbf{q}$ at seventh order in J/T, implying no wave-vector selection. At eighth order in the expansion, $\lambda_1(\mathbf{q})$ takes the form

$$\lambda_1(\mathbf{q}) = \lambda_1(J/T) + 2\chi_{\text{hex}} F(\mathbf{q}) , \tag{38}$$

with extrema at $\mathbf{q}=\mathbf{0}$, where $F(0)=4$, and at $\mathbf{q}_{\sqrt{3}}$, where $F(\mathbf{q}_{\sqrt{3}})=-2$. χ_{hex} is related to the sum of spin correlations around a hexagon,

$$\chi_{\text{hex}} = \langle \mathbf{S}_0\cdot(\mathbf{S}_1-\mathbf{S}_2+\mathbf{S}_3-\mathbf{S}_4+\mathbf{S}_5-\mathbf{S}_6)\rangle , \tag{39}$$

where the appropriate spin positions are labeled in Fig. 16. χ_{hex} should be averaged over all spins $\mathbf{S}_0$ and all four hexagons for each $\mathbf{S}_0$. Whether $\mathbf{q}=\mathbf{0}$ or $\sqrt{3}\times\sqrt{3}$ orderings are selected is determined by the sign of χ_{hex}. For $\chi_{\text{hex}}<0$ the $\sqrt{3}\times\sqrt{3}$ ordering wave vector is selected. We have calculated χ_{hex} by the MC method and compared it with the series-expansion result

$$\chi_{\text{hex}} = -\frac{8}{25}\left[\frac{J}{3T}\right]^8 + O\left\{\left[\frac{J}{3T}\right]^9\right\} . \tag{40}$$

The series-expansion approximation to χ_{hex} drops very rapidly near $T/J \approx \frac{1}{3}$ with the MC result, showing similar behavior at a lower temperature (Fig. 16). The inset shows the MC results at low temperature on a logarithmic temperature scale, where χ_{hex} is seen to remain negative definite down to the lowest temperatures simulated.

Harris, Kallin, and Berlinsky[18] have also calculated the uniform static susceptibility χ_u (not to be confused with χ_0) and compared it with the experiments of Aeppli *et al.*[36] They argue that previous estimates of the exchange constant J, based on Curie-Weiss law plots, were too large because the measured data were not really in the asymptotic regime. In Fig. 17 we show the series-expansion, MC, and Curie-Weiss law results for $(J\chi_u)^{-1}$. The agreement between the series-expansion and MC results is excellent for $T/J>1$. A fourth-order Padé approximate to the series has also been included and allows comparison to even lower temperatures. Harris, Kallin, and Berlinsky have speculated that the roughly linear temperature dependence of the exact theoretical result for $(J\chi_u)^{-1}$ extends to much lower temperatures and the MC data show that this is essentially correct. In the zero-temperature limit, the MC result for $(J\chi_u)^{-1}$ seems to approach 2, contrary to the measurements on $SrCr_{8-x}Ga_{4+x}O_{19}$ for which $(J\chi_u)^{-1}\to 0$ as $T\to 0$. The discrepancy may be the result of (1) the nonstoichiometry in $SrCr_{8-x}Ga_{4+x}O_{19}$, as nonmagnetic sites will locally relieve the frustration, (2) non-negligible coupling between planes along the crystallographic c axis, and/or (3) Cr^{3+} spins residing on the intervening triangular sheets between kagomé layers. These "extra" spins have so far

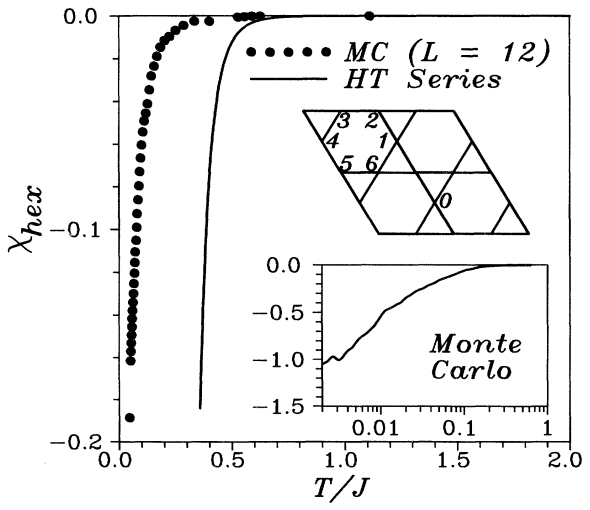

FIG. 16. Comparison of χ_{hex} as calculated from the series-expansion approximation, Eq. (37), and the MC method for $L=12$. The inset shows the MC result at lower temperatures on a logarithmic temperature scale. The spin-labeling scheme used in the definition of χ_{hex} in Eq. (39), is also shown.

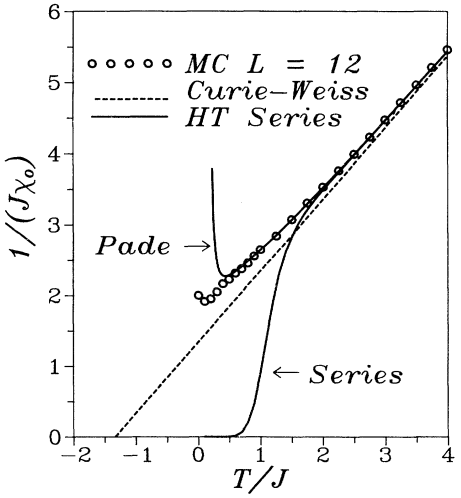

FIG. 17. Comparison of the Curie-Weiss, series expansion, and MC results for the inverse uniform static susceptibility.

received almost no attention in the literature concerning $SrCr_{8-x}Ga_{4+x}O_{19}$.

X. SUMMARY AND CONCLUSIONS

We have used the MC method to study magnetic ordering on the highly frustrated kagomé lattice. The ground state is highly degenerate, and any ordering that occurs must be due to thermal fluctuations which lift this degeneracy in the limit $T \to 0$. Obtaining a good statistical sampling of phase space, at very low temperatures with MC simulations, proved to be difficult, and results were averaged over many runs in an attempt to overcome this problem. From this work our conclusions are as follows.

(1) By studying the low-temperature behavior of the internal energy and entropy, we see evidence for the soft mode predicted by low-temperature expansions.[4] At temperatures above $\approx 0.01J$, the modes become renormalized and the soft mode disappears.

(2) The nematic (coplanar) and three-state Potts-like ordering susceptibilities χ_{n2} and χ_{C3} indicate the onset of coplanar three-state Potts-like ordering below $T/J=0.01$.

(3) The uniform and staggered chiral ordering susceptibilities χ_{n1} and χ_{n1}^{St} are much smaller than χ_{n2} or χ_{C_3} in the low-temperature regime. The growth of χ_{n1}^{St} as $T \to 0$, while χ_{n1} decreases, indicates a weak tendency toward local staggered chiral ordering.

(4) The nematic and three-state Potts correlation functions appear to be long range at low temperatures, as indicated by power-law decays with distance, while the chiral correlations remain strictly short range to within statistical errors. The Fourier transform of the chiral correlations $C_{n1}(q)$ has the appearance of a liquid-structure factor, indicating no long-range chiral order of any sort. Even relaxing a $\sqrt{3}\times\sqrt{3}$ ground-state configuration (which has chiral order) at temperatures as low as $T/J=0.0005$ resulted in short-range chiral order.

(5) In the low-temperature regime, a tendency toward $\sqrt{3}\times\sqrt{3}$ Néel ordering is observed in the order parameter $m_{\sqrt{3}}$. The $\sqrt{3}\times\sqrt{3}$ order parameter is shown to be strongly fluctuating, in that $\chi_{\sqrt{3}}$ apparently diverges as $T \to 0$, indicating criticality. The theory of finite-size scaling of the order parameter near a critical point has been applied to $m_{\sqrt{3}}$, yielding very rough estimates for the critical exponents. These results are all consistent with $T=0$ being a critical point.

(6) Warming runs from the $\mathbf{q}=\mathbf{0}$ ground state show a transition near $T/J \approx 0.008$, indicating metastability with respect to the $\sqrt{3}\times\sqrt{3}$ ground state.

(7) The $\sqrt{3}\times\sqrt{3}$ correlation function $C_{\sqrt{3}}(r)$ shows power-law decay below $T/J=0.01$, indicating a correlation length greater than the simulated lattice size. Whether or not this correlation length diverges as $T \to 0$ is impossible to prove using MC methods, but seems plausible.

(8) The low-temperature neutron-diffraction powder pattern shows weak reflections consistent with some degree of $\sqrt{3}\times\sqrt{3}$ ordering of the spins.

(9) Snapshots of the chiral order indicate chiral domains of various sizes. The domain walls are shown to cost zero internal energy and can also move without any cost in internal energy.

(10) The chiral domain structure is shown to map onto a triangular-lattice percolation problem at half filling if short-range chiral correlations are ignored. The triangular lattice at half filling is at its percolation threshold, implying that there is no natural length scale in chiral domain structure. Domains of all sizes can in principle exist.

(11) The effect of the chiral domains on the spin-spin correlations is to attenuate them with a power-law decay that describes the probability that any two spins, separated by a distance r, are in the same domain.

(12) Comparisons with some results from the high-temperature series expansion are made. The predicted behavior of the local susceptibility χ_{hex}, which governs wave-vector selection, as determined by the expansion, is shown to be correct with a renormalized temperature scale. The expansion result for the uniform susceptibility is confirmed, and the low-temperature limit $(J\chi_u)^{-1}=2$ is also reported.

We were unable to verify previous reports that true long-range $\sqrt{3}\times\sqrt{3}$ ordering takes place at $T \to 0$. True long-range $\sqrt{3}\times\sqrt{3}$ order implies the simultaneous existence of long-range staggered chiral ordering for which we have seen no evidence, possibly because of their very rapid decay with distance. Perfect chiral ordering is unstable toward the formation of chiral domain walls which cost zero internal energy but do provide a gain in entropy at low concentrations. At high concentrations the opposite should be true since soft modes in the neighborhood of a domain wall will be stiffened by the wall. Hence the question of true long-range order at $T=0$ as opposed to $T=0$ being a critical point will be decided by a subtle balance between the positive entropy of chiral domain walls and the soft-mode stiffening that they cause at high concentrations. It is remarkable that the $\sqrt{3}\times\sqrt{3}$ correlation function is rather insensitive to the chiral domain structure. Chiral domain walls simply increase the exponent in the expected zero-temperature power-law decay of $C_{\sqrt{3}}(r)$ with distance. The observed behavior (in our work) of the $\sqrt{3}\times\sqrt{3}$ order parameter, its fluctuations, the chiral domain structure, and the algebraic decay of the spin correlations all suggest that $T=0$ is a critical point of the classical Heisenberg kagomé antiferromagnet, implying that the ordered moment at $T=0$ vanishes. Our observation of ordered moments is purely a finite-size effect, and we expect that they scale to zero as $L \to \infty$ [see Eq. (24)].

In light of our results, a number of interesting questions arise which are beyond the scope of this paper. For example, what are the critical properties; i.e., how do the various correlation lengths diverge? Also, how do quantum fluctuations affect the chiral domain structure? Insight gained from studying the kagomé-lattice antiferromagnets may be useful in understanding its three-dimensional analog, the pyrochlore lattice. Indeed, our results indicate that previous MC studies[16] of the pyrochlore Heisenberg antiferromagnet may not have extend-

ed to low enough temperatures to see thermal selection effects.

ACKNOWLEDGMENTS

We would like to thank Ian Affleck, Andrey Chubukov, Malcolm Collins, Michel Gingras, Christopher Henley, David Huse, Michael Plischke, Andrew Rutenberg, Eugene Shender, and Michael Wortis for useful discussions. We also thank Andrew Rutenberg for providing us with his data for the three-state Potts model correlations. Computer facilities were kindly made available to us by Jeff Dahn, Catherine Kallin, Peter Sutherland, and Nathan Weiss. This work has been funded by the Natural Sciences and Engineering Research Council of Canada (NSERC).

[1]J. M. Coey, Can. J. Phys. **65**, 1210 (1987).

[2]E. Rastelli, A. Tassi, and L. Reatto, Physica **97B**, 1 (1979); N. Read and S. Sachdev, Phys. Rev. Lett. **66**, 1773 (1991); S. Sachdev and N. Read, Int. J. Mod. Phys. B **5**, 219 (1991); M. P. Gelfand, R. R. P. Singh, and D. A. Huse, Phys. Rev. B **40**, 10 801 (1989).

[3]P. Chandra and P. Coleman, Phys. Rev. Lett. **66**, 100 (1991); P. Chandra, P. Coleman, and A. I. Larkin, J. Phys. C **2**, 7933 (1990).

[4]J. T. Chalker, P. C. W. Holdsworth, and E. F. Shender, Phys. Rev. Lett. **68**, 855 (1992).

[5]G. H. Wannier, Phys. Rev. **79**, 357 (1950).

[6]A. Dannielian, Phys. Rev. **133**, A1344 (1964); M. K. Phani, J. L. Lebowitz, and M. H. Kalos, Phys. Rev. B **21**, 4027 (1980); T. L. Polgreen, *ibid.* **29**, 1468 (1984); D. F. Styer, *ibid.* **32**, 393 (1985).

[7]J. Villian, R. Bidaux, J. P. Carton, and R. J. Conte, J. Phys. (Paris) **41**, 1263 (1980).

[8]P. W. Anderson, Science **235**, 1196 (1987); P. W. Anderson, G. Baskaran, Z. Zou, and T. Hsu, Phys. Rev. Lett. **58**, 2790 (1987); S. Kivelson, D. Rokhsar, and J. Sethna, Phys. Rev. B **35**, 8865 (1987).

[9]See, for example, A. V. Chubukov, Phys. Rev. B **44**, 392 (1991); F. Mila, D. Poliblanc, and C. Bruder, *ibid.* **43**, 7891 (1991), and references therein.

[10]P. W. Anderson, Mater. Res. Bull. **8**, 153 (1973); P. Fazekas and P. W. Anderson, Philos. Mag. **30**, 423 (1974); V. Kalmeyer and R. B. Laughlin, Phys. Rev. Lett. **59**, 2095 (1987); Phys. Rev. B **39**, 11 879 (1989).

[11]R. R. P. Singh and D. A. Huse, Phys. Rev. Lett. **68**, 1766 (1992).

[12]D. A. Huse and V. Elser, Phys. Rev. Lett. **60**, 2531 (1988).

[13]G. Baskaran, Phys. Rev. Lett. **63**, 2524 (1989).

[14]J. N. Reimers, A. J. Berlinsky, and A.-C. Shi, Phys. Rev. B **43**, 865 (1991).

[15]V. Elser, Phys. Rev. Lett. **62**, 2405 (1989).

[16]J. N. Reimers, Phys. Rev. B **45**, 7287 (1992).

[17]N. D. Mermin and H. Wagner, Phys. Rev. Lett. **17**, 1133 (1966).

[18]A. B. Harris, C. Kallin, and A. J. Berlinsky, Phys. Rev. B **45**, 2899 (1992).

[19]D. A. Huse and A. D. Rutenberg, Phys. Rev. B **45**, 7536 (1992).

[20]A. Chubukov, Phys. Rev. Lett. **69**, 832 (1992).

[21]C. L. Henley (unpublished).

[22]P. Chandra, P. Coleman, and I. Ritchey, J. Appl. Phys. **69**, 4974 (1991).

[23]S. Sachdev, Phys. Rev. B **45**, 12 377 (1992).

[24]D. S. Greywall and P. A. Busch, Phys. Rev. Lett. **62**, 1868 (1989); **65**, 2788 (1990); D. A. Greywall, Phys. Rev. B **41**, 1842 (1990).

[25]C. Broholm, G. Aeppli, G. P. Espinosa, and A. S. Cooper, J. Appl. Phys. **67**, 5799 (1990); Phys. Rev. Lett. **65**, 3173 (1990); A. P. Ramirez, G. P. Espinosa, and A. S. Cooper, *ibid.* **64**, 2070 (1990).

[26]J. E. Dutrizac and S. Kaiman, Can. Mineral. **14**, 151 (1976); J. Kubisz, Mineral. Pol. **1**, 47 (1970); A. Bonnin and A. Lecerf, C. R. Acad. Sci. Paris **262**, 1782 (1966).

[27]M. G. Townsend, G. Longworth, and E. Roudaut, Phys. Rev. B **33**, 4919 (1986).

[28]M. Leblanc, G. Ferey, P. Chevallier, Y. Calage, and R. De Pape, J. Solid State Chem. **47**, 53 (1983); M. Leblanc, R. De Pape, and G. Ferey, Solid State Commun. **58**, 171 (1986).

[29]J. F. Fernandez and T. S. J. Streit, Phys. Rev. B **25**, 6910 (1982).

[30]A. M. Ferrenberg, and R. H. Swendsen, Phys. Rev. Lett. **61**, 2635 (1988); **63**, 1195 (1988); Comput. Phys. **3**, 101 (1989); E. P. Münger and M. A. Novotny, Phys. Rev. B **43**, 5773 (1991).

[31]E. Brézin and J. Zinn-Justin, Phys. Rev. B **14**, 3110 (1976); S. H. Shenker and J. Tobochnik, *ibid.* **22**, 4462 (1980); P. Kopietz and S. Chakravarty, *ibid.* **40**, 4858 (1989).

[32]M. E. Fisher, in *Critical Phenomena,* edited by M. S. Green (Academic, New York, 1971); M. E. Fisher and M. N. Barber, Phys. Rev. Lett. **28**, 1516 (1972); D. P. Landau, Phys. Rev. B **13**, 2997 (1976); **14**, 225 (1976).

[33]H. Kawamura, J. Phys. Soc. Jpn. **58**, 584 (1989); **56**, 474 (1987); J. N. Reimers, J. E. Greedan, and M. Björgvinsson, Phys. Rev. B **45**, 7295 (1992).

[34]J. N. Reimers, Phys. Rev. B **46**, 193 (1992).

[35]D. Stauffer, Phys. Rep. **54**, 1 (1979), D. Stauffer, *Introduction to Percolation Theory* (Taylor & Francis, London, 1985); M. L. Plischke and B. Bergersen, *Equilibrium Statistical Mechanics* (Prentice-Hall, Englewood Cliffs, NJ, 1989), p. 312.

[36]G. Aeppli, C. Broholm, A. P. Ramirez, G. P. Espinosa, and A. S. Cooper, J. Magn. Magn. Mater. **90&91**, 255 (1990).